Precision Measurement of the Neutral Pion Lifetime

I. Larin,[1,2] Y. Zhang,[3] A. Gasparian*,[4] L. Gan†,[5] R. Miskimen†,[2] M. Khandaker†,[6] D. Dale†,[7] S. Danagoulian,[4] E. Pasyuk,[8] H. Gao,[3] A. Ahmidouch,[4] P. Ambrozewicz,[4] V. Baturin,[8] V. Burkert,[8] A. Deur,[8] A. Dolgolenko,[1] D. Dutta,[9] G. Fedotov,[10] J. Feng,[5] S. Gevorkyan,[11] A. Glamazdin,[12] L. Guo,[13] E. Isupov,[10] M.M Ito,[8] F. Klein,[14] S. Kowalski,[15] M. Kubantsev,[16] A. Kubarovsky,[8] V. Kubarovsky,[8] D. Lawrence,[8] H. Lu,[17] V. Matveev,[1] B. Morrison,[18] A. Micherdzinska,[19] I. Nakagawa,[20] K. Park,[8] R. Pedroni,[4] W. Phelps,[21] D. Protopopescu,[22] D. Rimal,[13] C. Salgado,[6] A. Shahinyan,[23] D. Sober,[14] S. Stepanyan,[8] V.V. Tarasov,[1] S. Taylor,[8] A. Vasiliev,[24] M. Wood,[2] L. Ye,[9] and B. Zihlmann[8]

(PrimEx-II Collaboration)

[1] *Alikhanov Institute for Theoretical and Experimental Physics NRC "Kurchatov Institute", Moscow, 117218, Russia*
[2] *University of Massachusetts, Amherst, MA 01003, USA*
[3] *Duke University and Triangle University Nuclear Lab, Durham, MC 27708, USA*
[4] *North Carolina A&T State University, Greensboro, NC 27411, USA*
[5] *University of North Carolina Wilmington, Wilmington, NC 28403, USA*
[6] *Norfolk State University, Norfolk, VA 23504, USA*
[7] *Idaho State University, Pocatello, ID 83209, USA*
[8] *Thomas Jefferson National Accelerator Facility, Newport News, VA 23606, USA*
[9] *Mississippi State University, Mississippi State, MS 39762, USA*
[10] *Moscow State University, Moscow 119991, Russia*
[11] *Joint Institute for Nuclear Research, Dubna 141980, Russia*
[12] *Kharkov Institute of Physics and Technology, Kharkov, 310108, Ukraine*
[13] *Florida International University, Miami, FL 33199, USA*
[14] *The Catholic University of America, Washington, DC 20064, USA*
[15] *Massachusetts Institute of Technology, Cambridge, MA 02139, USA*
[16] *Northwestern University, Evanston, IL 60208, USA*
[17] *Carnegie Mellon University, Pittsburgh, PA 15213, USA*
[18] *Arizona State University, Tempe, AZ 85281, USA*
[19] *George Washington University, Washington, DC 20064, USA*
[20] *University of Kentucky, Lexington, KY 40506, USA*
[21] *Christopher Newport University, Newport News, VA 23606, USA*
[22] *Glasgow University, Glasgow G12 8QQ, UK*
[23] *Yerevan Physics Institute, Yerevan 0036, Armenia*
[24] *NRC "Kurchatov Institute", Institute for High Energy Physics, Protvino 142281, Russia*

(Dated: July 11, 2019)

Symmetries, and most importantly the phenomena of broken symmetries, play critical roles in the properties of matter. In particular, two fundamental symmetries are directly involved both in the existence and in the lifetime of the neutral pion (π^0): the axial and left-right chiral symmetries. The explicit breaking of the axial symmetry, due to quantum fluctuations, gives rise to one of the intriguing effects in nature, the so-called axial (or chiral) anomaly. This process is purely responsible for the π^0 decay into two photons, yielding its unusually short lifetime. The PrimEx collaboration performed a new experiment at Jefferson Lab (JLab) to measure the $\pi^0 \to \gamma\gamma$ decay width with a record precision to test the chiral anomaly. The differential cross sections for π^0 photoproduction at forward angles have been measured on two targets, ^{12}C and ^{28}Si at incident photon energies of 4.45 – 5.30 GeV. The $\pi^0 \to \gamma\gamma$ decay width was extracted from the measured cross sections, resulting in $\Gamma(\pi^0 \to \gamma\gamma) = 7.798 \pm 0.056\,(\text{stat.}) \pm 0.109\,(\text{syst.})$ eV. Its 1.57% total uncertainty improves approximately by a factor of two over the previously published most precise result of $\Gamma(\pi^0 \to \gamma\gamma)$. Combining this result with the one from an earlier JLab experiment, the weighted average is: $\Gamma(\pi^0 \to \gamma\gamma) = 7.802 \pm 0.052\,(\text{stat.}) \pm 0.105\,(\text{syst.})$ eV, defining the new lifetime: $\tau = 8.337 \pm 0.0556(stat.) \pm 0.1122(syst.) \times 10^{-17} s$. Our final result with its 1.50% total uncertainty represents the most accurate measurement of this fundamental quantity to date. It confirms firmly the chiral anomaly in QCD, and presents challenges to existing theory corrections to the anomaly.

PACS numbers: 11.80.La, 13.60.Le, 25.20.Lj

The lightest pseudoscalar hadrons, the π mesons, were first proposed by Yukawa [1] as the intermediaries of the nuclear interactions. They result from a profound phenomenon in the contemporary physics of the strong interaction described by Quantum Chromodynamics (QCD), the theory of quarks and gluons which are the fundamental constituents of hadrons. The basic symmetries of the classical world are at the origin of the most fundamental conservation laws and, via quantum gauge theories, of our modern understanding of Nature. Although gener-

*spokesperson, corresponding author, gasparan@jlab.org
†spokesperson

ally, classical symmetries are respected in the quantum realm, it was realized several decades ago that it may not be always so due to so-called "anomalies". Arguably, the most famous one is the axial anomaly, without which $\pi^0 \to \gamma\gamma$ decay would not exist. This anomaly is represented by truly unique graphs in perturbative quantum field theory that do not need renormalization, thereby enabling an absolute prediction from QCD – the π^0 lifetime – while generally, QCD can predict analitically only relative features and needs either experimental data, models or numerical lattice inputs, to anchor its relative predictions. Thus, verifying experimentally with the highest accuracy this remarkable phenomenon, as reported in this article, is a unique and absolute test of quantum field theory and of symmetry breaking by pure quantum effects [2].

The fact that the three light quarks, u, d and s, have much smaller masses than the energy scale of QCD gives rise to an approximate chiral flavor symmetry consisting of chiral left-right and axial symmetries. The chiral symmetry is spontaneously broken by the non-perturbative dynamics of QCD which leads to the condensation of quark pairs, the $\langle \bar{q}q \rangle$ condensate. This phenomenon is responsible for the observed octet of light pseudoscalar mesons in Nature. The π^0, the subject of this work, being one of them. The axial symmetry is explicitly broken by the quantum phenomenon known as the axial (or chiral) anomaly [3], originating from the quantum fluctuations of the quark and gluon fields. The chiral anomaly drives the π^0 decay into two photons with no free parameters in the predicted decay width [4]:

$$\Gamma(\pi^0 \to \gamma\gamma) = \frac{m_{\pi^0}^3 \alpha^2 N_c^2}{576\pi^3 F_{\pi^0}^2} = 7.750 \pm 0.016\, eV, \qquad (1)$$

where α is the fine-structure constant, m_{π^0} is the π^0 mass, $N_c = 3$ is the number of colors in QCD, and F_{π^0} is the pion decay constant, $F_{\pi^0} = 92.277 \pm 0.095\,\mathrm{MeV}$ extracted from the charged pion weak decay [5].

The study of corrections to the chiral anomaly has been mainly done with Chiral Perturbation Theory (ChPT), with the three light flavors. The dominant corrections are the result of meson state mixing due to the differences between the quark masses. For the π^0, its mixing with the η and η' states comes from the isospin breaking due to $m_u < m_d$, an effect that is calculable in a global analysis of the three neutral mesons [6]. Goity *et al.* [6] calculated the $\Gamma(\pi^0 \to \gamma\gamma)$ width in a combined framework of ChPT and $1/N_C$ expansion up to $\mathcal{O}(p^6)$ and $\mathcal{O}(p^4 \times 1/N_C)$ in the decay amplitude. Their result, $\Gamma(\pi^0 \to \gamma\gamma) = 8.10 \pm 0.08\,\mathrm{eV}$ with $\sim$1% estimated uncertainty is about 4.5% higher than the prediction of chiral anomaly. Another Next-to-Leading-Order (NLO) calculation in ChPT was performed by Ananthanarayan *et al.* [7] which resulted in $8.06 \pm 0.06\,\mathrm{eV}$. The only Next-to-Next-to-Leading-Order (NNLO) calculation for the decay width was performed by Kampf *et al.* [8] yielding a similar result, $8.09 \pm 0.11\,\mathrm{eV}$. Ioffe et al. [9] calculated the corrections to the chiral anomaly in the framework of QCD using dispersion relations and sum rules. Their result, $7.93 \pm 0.12\,\mathrm{eV}$ is about 2% lower than the ChPT predictions. The fact that all That these calculations performed by different methods differ from the chiral anomaly by the few percents with accuracy of about one percent, makes the precise measurement of the $\pi^0 \to \gamma\gamma$ width a definitive low-energy test of QCD.

In the past decades, there have been extensive efforts to measure the π^0 radiative decay width using three experimental methods: the Primakoff, the direct, and the collider methods (described in Sec. of Supplemental materials). The current Particle Data Group (PDG) value of $\pi^0 \to \gamma\gamma$ decay width is $7.63 \pm 0.16\,\mathrm{eV}$ [5]. It is the average of five measurements, two Primakoff types: Cornell [12] with $7.92 \pm 0.42\,\mathrm{eV}$, and PrimEx-I [11] with $7.82 \pm 0.14\,(\mathrm{stat.}) \pm 0.17\,(\mathrm{syst.})\,\mathrm{eV}$, one direct measurement: CERN [13] with $7.25 \pm 0.18\,(\mathrm{stat.}) \pm 0.14\,(\mathrm{syst.})\,\mathrm{eV}$, one collider measurement: DESY [14] with $7.7 \pm 0.72\,\mathrm{eV}$, and the fifth one is from the radiative pion decay: $\pi^+ \to e^+\nu\gamma$, using the conserved vector current hypothesis to relate the π^+ decay to the $\pi^0 \to \gamma\gamma$ one, PIBETA [15] with $7.74 \pm 1.02\,\mathrm{eV}$. The result from the PrimEx-I experiment [11] improved the previous PDG value by a factor of two-and-a-half and confirmed the validity of the chiral anomaly at the few percent level. However, there is a 6% discrepancy between the two most precise experiments included in the PDG average, the CERN direct [13] and PrimEx-I Primakoff [11]. Furthermore, the accuracy of the PDG average is still not adequate to test the theory corrections to the prediction of the anomaly. The PrimEx-II experiment was condacted at Jefferson Laboratory (JLab) to address these issues.

Both PrimEx-I and PrimEx-II experiments have been performed in Hall B at JLab using the existing high resolution photon tagging facility [16] and a specifically developed state-of-the-art hybrid electromagnetic calorimeter, HyCal [17] (see Fig. 3 in the Supplemental section). PrimEx-I achieved a total uncertainty of 2.8% in the extracted width $\Gamma(\pi^0 \to \gamma\gamma)$ [11]. The PrimEx-II experiment aimed to significantly increase the statistics and improve the systematic uncertainties to reach the percent level accuracy. The following was implemented to increase the statistics by a factor of seven: (a) the accepted energy interval of the tagged photons was increase by 50%; (b) thicker solid targets were used: 8% radiation length (r.l.) ^{12}C and 10% r.l. ^{28}Si; (c) the performance of the data acquisition (both at electronics and software levels) was upgraded to increase the data taking rate by a factor of five. The systematic uncertainties were reduced thanks to several improvements: (a) the central part of the HyCal (about 400 modules) was equipped with individual TDCs for better rejection of time accidental events; b) the trigger for the experiment was simplified by using only events with a total deposited energy above 2.5 GeV in the HyCal calorimeter; (c) a set of new

12 horizontal scintillator veto counters was added for a better rejection of charged particles in HyCal; (d) the distance between the calorimeter and target was reduced to 7 m, allowing for a better geometrical acceptance between 1.0° to 2.0° in the π^0 production angles. It provided a better separation of the nuclear coherent and incoherent production terms from the Primakoff process in the measured cross sections (see Supplemental materials and eq. (1)). In addition, the improved running conditions (beam intensity and position stability, etc.) by the CEBAF accelerator allowed for a significant reduction of the beam-related systematic uncertainties. Using an intermediate-atomic-number target, ^{28}Si, in combination with a low-atomic-number target, ^{12}C, allowed more effective control of systematic uncertainties related to the extraction of the Primakoff contribution (two production amplitudes and four production terms for this process are described in the Supplemental materials). Similar to the PrimEx-I experiment [11], the combination of the photon tagger with its well-defined photon energy and timing together with the HyCal calorimeter defined the event selection criteria (see Supplemental materials).

The event yield (the number of elastically produced π^0 events for each angular bin) was extracted using the kinematic constraints described in the Supplemental materials, and by fitting the experimental two-photon invariant mass spectra ($M_{\gamma\gamma}$) to subtract the background contributions. Two independent analysis methods, the "constrained" and "hybrid" mass methods (described in Supplemental material), were used to extract the event yield for the PrimEx-II experiment. The two methods (integrated over the angular range of $\theta_\pi = 0^\circ - 2.5^\circ$ and for the incident energies $E_\gamma = 4.45 - 5.30$ GeV) agree with each other. The total integrated statistics was about 83,000 π^0 events on ^{12}C and 166,000 on ^{28}Si targets, a factor of six increase compere to PrimEx-I. This reduced the statistically limited part of the systematic uncertainties in the yield extraction process. Combining the two analysis methods with the partially independent systematics further reduced the systematic uncertainty to 0.80%. This includes the uncertainty in the physics background subtraction, 0.10%, mostly from ω mesons photoproduction. High precision monitoring of the photon beam flux during the entire data taking process is one of the challenging tasks for this type of experiment [18]. As described in the Supplemental materials, a photon tagger is used for measurements of the photon beam flux, a total absorption counter (TAC) for periodic measurements of the absolute tagging ratios, and a pair-spectrometer (PS) for continuous monitoring of the relative tagging ratios and tagger stability. The stability of the beam parameters (position, width, and frequency of interruptions) was far better than in PrimEx-I. That, and more frequent TAC measurements, led to a better measurement of the photon flux, 0.80%. Different measurement methods allowed to achieve sub-percent accuracy for the uncertainty in the number of target nuclei per cm^{-2}: less than 0.10% for ^{12}C and 0.35% for ^{28}Si targets [19, 20]. The geometrical acceptances and resolutions of the experimental setup have been calculated by a GEANT-based Monte Carlo simulation package. The contributed uncertainty in the extracted cross sections from this part is estimated to be 0.55%.

The extracted differential cross sections of π^0 photoproduction on both ^{12}C and ^{28}Si are shown in Fig. 1. They are integrated over the incident photon beam energies of 4.45 to 5.30 GeV (with the weighted average value of 4.90 GeV). The fit results for the four contributing processes to forward production: Primakoff, Nuclear coher-

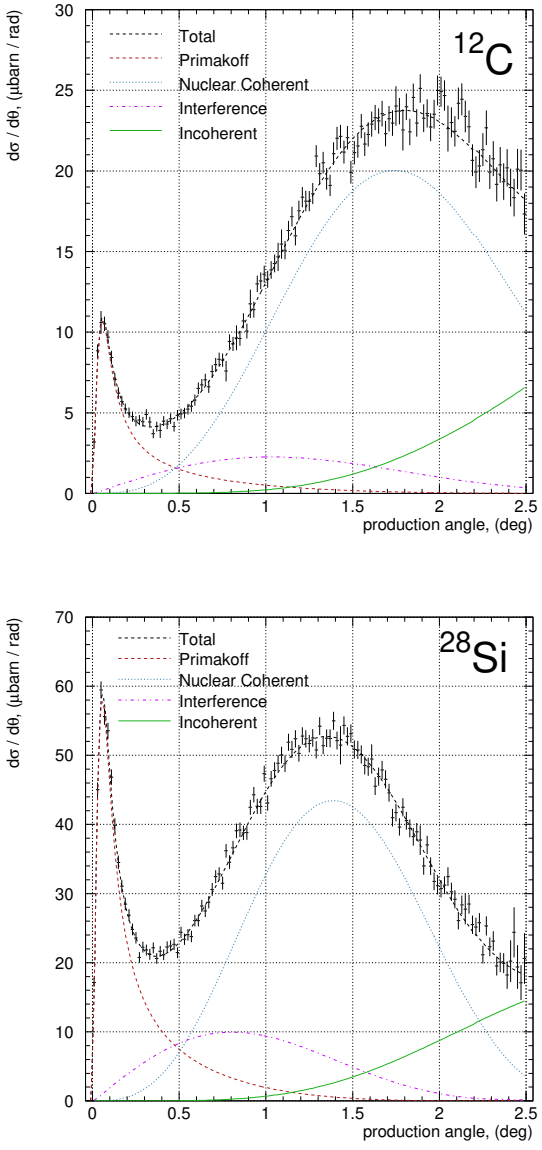

FIG. 1: Experimental differential cross section as a function of the π^0 production angle for ^{12}C (top) and ^{28}Si (bottom) together with the fit results for the different physics processes (see insert and text for explanations).

ent, Interference between them, and Nuclear incoherent are also shown(see the Supplemental materials).

The $\pi^0\to\gamma\gamma$ decay width was extracted by fitting the experimental differential cross sections to the theoretical terms of four contributing processes (see Eq. (1) in the Supplemental section), convoluted with the angular resolution, experimental acceptances and folded with the measured incident photon energy spectrum. The effect of final state interactions between the outgoing pion and the nuclear target, and the photon shadowing effect in nuclear matter must be accurately included in the theoretical cross sections for the precise extraction of the Primakoff term, and therefore, the $\Gamma(\pi^0\to\gamma\gamma)$ [21]. Two groups analyzed the data using different methods. They extracted $\Gamma(\pi^0\to\gamma\gamma)$ from their cross sections using similar fitting procedures (shown in Table I in the Supplemental section). Thus, for the same target, the statistical and part of the systematic uncertainties from two analysis groups are correlated. This was accounted for when the two results were combined. Results from the individual targets were combined using the weighted average method: $\Gamma(\pi^0\to\gamma\gamma) = 7.763\pm0.127\,(\text{stat.})\pm0.117\,(\text{syst.})\,\text{eV}$ for ^{12}C, and $7.806\pm0.062\,(\text{stat.})\pm0.109\,(\text{syst.})\,\text{eV}$ for ^{28}Si. The results from the two different targets were then combined together to give the final result: $\Gamma(\pi^0\to\gamma\gamma) = 7.798\pm0.056\,(\text{stat.})\pm0.109\,(\text{syst.})\,\text{eV}$, with a total uncertainty of 1.57% (Fig. 2).

To check the sensitivity of the extracted decay width on the theory parameters (nuclear matter density, nuclear radii, photon shadowing parameter, π^0N total cross section, etc.) their values were changed by several sigma and refitted to obtain new decay widths. In this way, the two main contributors to the systematic uncertainties were found to be the nuclear radii and the photon shadowing parameter ([24], Boyarski:1969kh). The nuclear coherent process dominating at larger angles for both targets, was determined with a high precision (see Fig. 1). This information was used to extract the nuclear radii for our targets. To do so, the radii were varied about the experimental values from electron scattering data [22, 23], known within 0.6%. Then, the best values for the nuclear radii were defined from minimizing the resulting χ^2 distributions. Our extracted results for the nuclear radii are: $2.457\pm0.047\,\text{fm}$ for ^{12}C and $3.073\pm0.018\,\text{fm}$ for ^{28}Si. They agree with the radii extracted from electron scattering [22, 23]. The shadowing parameter was extracted with a similar procedure. The extracted value is: $\xi = 0.30\pm0.17$, agreeing with two previous measurements: 0.25 from [24] and 0.31 ± 0.12 from [25]. Variation of this parameter within a $3\,\sigma$ interval gave only a 0.30% uncertainty in the extracted $\Gamma(\pi^0\to\gamma\gamma)$ (correlated for two targets). Our systematic uncertainties are summarized in Table II in the Supplemental section.

For both PrimEx-I and PrimEx-II the validity of the experimental uncertainties has been verified by periodically measuring the Compton cross sections of the same nuclear targets. Our measured Compton cross sections agree with the theoretical simulations of this well-known QED process within 1.7%. These results will be published separately [26].

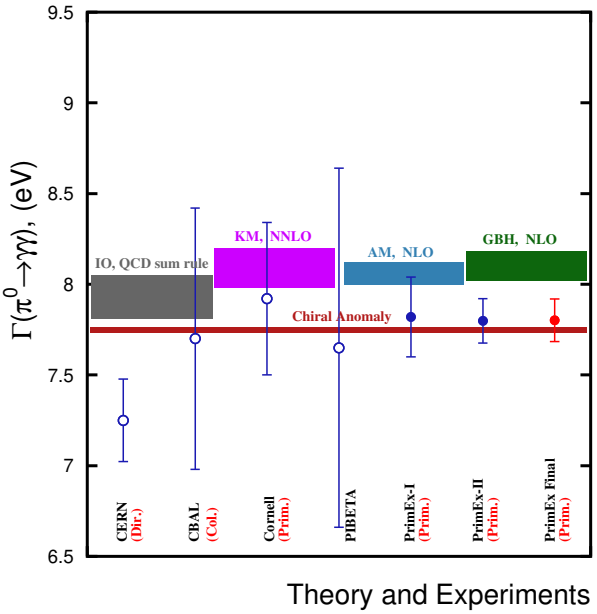

FIG. 2: Theoretical predictions and experimental results of the $\pi^0\to\gamma\gamma$ decay width. Theory: chiral anomaly [3] (dark red band); IO, QCD sum rule [9] (gray band); KM, ChPT NNLO [8] (magneta band); AM, ChPT NLO [7] (blue band); GBH, ChPT NLO [6] (green band). Experiments included in the current PDG [5]: CERN direct [13]; Crystal Ball collider [14]; Cornell Primakoff [12]; PIBETA [15]; PrimEx-I [11]. Our new results: PrimEx-II and the PrimEx Combined.

In combining results from the two experiments, correlations between different systematic uncertainties have been accounted for. The weighted average final result for the $\pi^0\to\gamma\gamma$ decay width from the two PrimEx experiments is $7.802\pm0.052\,(\text{stat.})\pm0.105\,(\text{syst.})\,\text{eV}$ (shown in Fig. 2), defining the new lifetime: $\tau = 8.337\pm0.0556(stat.)\pm0.1122(syst.)\times10^{-17}s$. With 1.50% total uncertainty, it is the most precise measurement of the $\Gamma(\pi^0\to\gamma\gamma)$, and as a single experimental result, firmly confirms the prediction of the chiral anomaly in QCD at the percent level. Also, as seen from Fig. 2, our result disagrees with theoretical corrections to the anomaly at the two standard deviation level.

We reported in this article on the most precise measurement of the $\pi^0\to\gamma\gamma$ decay width, which directly definse its lifetime. It proceeds from the axial anomaly, a remarkable quantume phenomenon whose study is of prime importance to fundamental physics [2]. Our result validates its prediction, one of the rare absolute analitical predictions of QCD. The anomaly, which historically has lead to the concept of QCD's color charge, continues to

teach us about the most fundamental aspects of Nature e.g. by strictly constraining physics beyond the Standard Model or enabling the unique opportunity of measuring quark masses ratios. Actually, light quark masses are yet unmeasured and it was even debated either they are in fact observable. Measurement of the ratios is now underway at JLab as the natural continuation of the PrimEx program [27].

We are grateful to the Accelerator and Physics Divisions at Jefferson Lab which made these experiments possible. We thank the Hall B engineering and physics staff for their critical contributions in all stages of these experiments. Theoretical support provided by Jose Goity throughout this project is gratefully acknowledged. This project was supported in part by the National Science Foundation under a Major Research Instrumentation grant (PHY-0079840). The Jefferson Science Associates, LLC operates Thomas Jefferson National Accelerator Facility under contract No. AC05-06OR23177 during this work.

[1] H. Yukawa Proc. Math. Soc. Jpn. 17:48 (1935)
[2] S. Weinberg, "The quantum theory of fields", Cambridge University Pr. (1996), v.2
[3] J.S.Bell and R.Jaciw, Nuovo Cimento A **60**, 47 (1969); S.L.Adler, *Phys. Rev.* **177**, 2426 (1969).
[4] A.M. Bernstein and B.R. Holstein, Rev. Mod. Phys. **85**, 49 (2013).
[5] M. Tanabashi *et al.*, Phys. Rev. D **98**, 030001 (2018).
[6] J. L. Goity, A.M. Bernstein, B.R. Holstein, *Phys. Rev. D* **66**, 076014 (2002).
[7] B. Ananthanarayan and B. Moussallam, *JHEP* **0205**, 052 (2002).
[8] K. Kampf and B. Moussallam, *Phys. Rev. D* **79**, 076005 (2009).
[9] B. L. Ioffe and A. G. Oganesian, *Phys. Lett.* B **647**, 389 (2007).
[10] H. Primakoff, *Phys. Rev.*, 81:899, 1951.
[11] I. Larin, *et al.*, *Phys.Rev.Lett.*, 106:162303, 2011.
[12] A. Browman *et al.*, Phys. Rev. Lett. **33**, 1400 (1974).
[13] H. W. Atherton *et al.*, Phys. Lett. **B158**, 81 (1985).
[14] D. Williams *et al.*, Phys. Rev., D38:1365, 1988.
[15] M. Bychkov *et al.*, Phys. Rev. Lett. **103**, 051802 (2009).
[16] D. I. Sober, *et al.*, Nucl. Instrum. Meth. A **440**, 263 (2000).
[17] A. Gasparian Proc. XI Int. Conf. Calorim. Part. Phys. 1:109 (2004).
[18] A. Teymurazyan, *et al.*, Nucl. Instrum. and Methods A **767**, 300 (2014).
[19] P. Martel *et al.*, Nucl. Instr. and Meth.**A612**, 46 (2009).
[20] C. Harris, R. Miskimen `http://www.jlab.org/primex_notes/SiTarget.pdf`.
[21] S. Gevorkyan, *et al.*, Phys. Rev. **C80**, 055201 (2009); Phys. Part. Nucl. Lett. 9, 3 (2012); arXiv:0908.1297 [hep-ph].
[22] H. De Vries, C. W. De Jager and C. De Vries, Atom. Data Nucl. Data Tabl. **36**, 495 (1987).
[23] E. A. J. M. Offermann, *et al.*, *Phys. Rev.* C **44**, 1096 (1991).
[24] W. T. Meyer, *et al.*, *Phys. Rev. Lett.*, **28**, 1344 (1972).
[25] A. Boyarski, *et al.*, *Phys. Rev. Lett.* **23**, 1343 (1969).
[26] P. Ambrozewicz, *et al.*, arXiv:1903.05529v2 [nucl-ex].
[27] A. Gasparian, *et al.*, JLab Proposal E12-10-011. (`http://www.jlab.org/exp_prog/proposals/10/PR12-10-011.pdf`)

SUPPLEMENTAL MATERIALS

Experimental Methods

Three major experimental methods have been used in the past to extract the π^0 lifetime (or the $\pi^0 \to \gamma\gamma$ decay width): (1) the direct method; (2) the Primakoff method and; (3) collider experiments. In the direct method the distribution of the decay time is extracted by measuring the decay lengths of π^0 mesons. Since the π^0 lifetime is rather short ($\sim 10^{-16}$ s), to have measurable distances in these experiments highly relativistic π^0's are produced and used [13] (the third experimental data point in Fig. 2). The Primakoff method is an indirect method using the photoproduction of π^0's at forward angles in the Coulomb field of a heavy nucleus [10]. This is essentially a time-reversed process of the $\pi^0 \to \gamma\gamma$ decay reaction, where the π^0's are being produced by "fusing" one real photon from the beam with a semi-real (having low virtuality) photon from the electromagnetic field of the nucleus. Several Primakoff type experiments have been performed in the past, before the PrimEx experiments. Typical uncertainties of these experiments (three were included in the PDG averaging before the publication of our PrimEx-I results) are in the 5% to 11% range. Only one Primakoff-experiment performed at Cornell in 1974 [12] (other than PrimEx-I) is included in the current PDG averaging [5] (the first experimental data point in Fig. 2). In collider experiments a similar process is used for the production of π^0's from the electromagnetic field of electron and positron beams: $e^+e^- \to e^+e^-\pi^0$. In these experiments the incident e^+ and e^- scatter in forward directions (undetected) to provide two semi-real photons for the π^0 production, which consequently are detected by their $\pi^0 \to \gamma\gamma$ decay channel [14] (the second experimental data point in Fig. 2).

In general, in high energy photoproduction experiments at small angles the π^0's can be produced by two different elementary mechanisms: the Primakoff process (one photon exchange), T_{Pr}, and the strong process (hadron exchange), T_S. These amplitudes contribute both coherently, as well as incoherently in the π^0 photoproduction process. Therefore, the cross section of this process can be expressed by four terms [11, 21]: Primakoff (Pr), nuclear coherent (NC), interference between strong and Primakoff amplitudes (Int), and nuclear incoherent (NI):

$$\begin{aligned} \frac{d\sigma}{d\Omega} &= \mid T_{Pr} + e^{i\varphi} T_S \mid^2 + \frac{d\sigma_{_{NI}}}{d\Omega} \\ &= \frac{d\sigma_{_{Pr}}}{d\Omega} + \frac{d\sigma_{_{NC}}}{d\Omega} + \frac{d\sigma_{_{Int}}}{d\Omega} + \frac{d\sigma_{_{NI}}}{d\Omega}, \end{aligned} \quad (1)$$

where φ is the relative phase between the Primakoff and the strong amplitudes. The Primakoff cross section is proportional to the π^0 decay width, the primary focus of this experiment [12]:

$$\frac{d\sigma_{_{Pr}}}{d\Omega} = \Gamma(\pi^0 \to \gamma\gamma) \frac{8\alpha Z^2}{m^3} \frac{\beta^3 E^4}{Q^4} |F_{EM}(Q)|^2 \sin^2\theta_\pi, \quad (2)$$

where Z is the atomic number; m, β, θ_π are the mass, velocity and production angle of the pion; E is the energy of the incident photon; Q is the four-momentum transfer to the nucleus; $F_{EM}(Q)$ is the nuclear electromagnetic form factor, corrected for the final state interactions (FSI) of the outgoing pion. The FSI effects for the photoproduced pions, as well as the photon shadowing effect in nuclear matter, need to be accurately included in the cross sections before extracting the Primakoff amplitude. To achieve this, and to calculate the NC and NI cross sections, a full modern theoretical description based on the Glauber method was developed in our collaboration in the past fifteen years, providing an accurate calculation of these processes in both light and heavy nuclei [21]. These simulation methods have been used in our fitting procedures to extract the $\pi^0 \to \gamma\gamma$ decay width from the experimental differential cross sections.

Experimental setup

In order to make a significant improvement in the accuracy of the Primakoff type of experiments and reach the one percent level goal, we have implemented three basic improvements in the experimental technique (see Fig. 3). A tagged photon beam was used for the first time, allowing critical improvements in the background separation and the determination of the photon flux. We also replaced the traditional Pb-glass based electromagnetic calorimeter, used in the previous experiments, with a newly developed $PbWO_4$ crystal based multichannel, high resolution and large acceptance electromagnetic calorimeter (HyCal) [17]. This improved the energy and coordinate reconstruction of photons from the $\pi^0 \to \gamma\gamma$ decay by a factor of two and a half, allowing a more precise event selection in the experiment. In addition, the cross sections of two well-known electromagnetic (QED) processes, the Compton scattering and the e^+e^- pair production from the same experimental target, were periodically measured to verify the validity of the experimental cross sections and their estimated systematic uncertainties.

Tagged photons with known timing and energy [16] were incident on two 5% r.l. targets of ^{12}C and ^{208}Pb for the PrimEx-I and 8% r.l. ^{12}C and 10% r.l. ^{28}Si targets for the PrimEx-II experiments [19, 20]. The photon relative tagging efficiencies were continuously measured during the experiment with a e^+e^- pair spectrometer (PS) consisting of a $\sim$1.7 T·m large aperture dipole magnet and two telescopes of scintillating counters located downstream of the targets. The absolute normalization of the photon beam was measured periodically during the experiment with a total absorp-

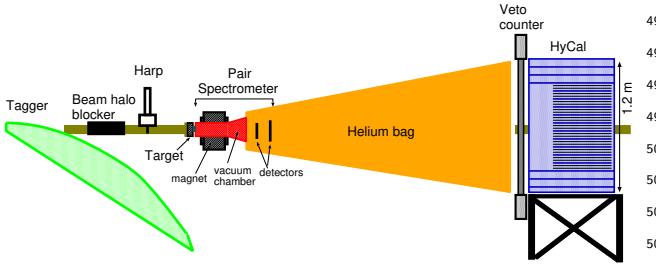

FIG. 3: Schematic view of the PrimEx-II experimental setup (not to scale, see the text for description of individual detectors and components).

tion counter (TAC), inserted in the beam line just behind the HyCal calorimeter (not shown in Fig. 3). During these measurements the intensity of the photon beam was lowered to up to 70 pA [18]. The decay photons from $\pi^0 \to \gamma\gamma$ were detected in a multichannel hybrid electromagnetic calorimeter (HyCal) [17] located 7.5 m downstream from the targets to provide a large geometrical acceptance of $\pi^0 \to \gamma\gamma$ events ($\sim$70%). The HyCal calorimeter consists of 1152 $PbWO_4$ crystal shower detectors (each with $2.05 \times 2.05 \times 18.0\,\mathrm{cm}^3$) in the central part, surrounded by 576 lead glass Cherenkov counters ($3.82 \times 3.82 \times 45.0$,$\mathrm{cm}^3$). Four crystal detectors were removed from the central part of the calorimeter ($4.1 \times 4.1\,\mathrm{cm}^2$ hole in size) for passage of the high intensity ($\sim 10^7\,\gamma$/s) incident photon beam through the calorimeter [17]. Twelve 5-mm-thick scintillator counters, located in front of HyCal, provided rejection of charged particles and effectively reduced the background in the experiment. For the PrimEx-II experiment a similar set of scintillator counters had been added to increase the rejection efficiency. To minimize the decay photon conversion in air, the space between the PS magnet to HyCal was enclosed by a helium bag at atmospheric pressure. The photon beam's position stability was continuously monitored during the experiment by an X-Y scintillating-fiber detector located downstream of HyCal (not shown in Fig. 3). For the PrimEx-I experiment the experimental trigger was formed by requiring coincidences between the photon tagger in the upper energy interval (4.9 – 5.5 GeV) and HyCal with a total deposited energy greater than 2.5 GeV. The trigger condition for the second, PrimEx-II experiment was simplified by requiring only signal from HyCal with the same total energy deposition.

Data analysis

A typical two-dimensional distribution (elasticity *vs.* $M_{\gamma\gamma}$) of experimental events with two or more photons in the HyCal calorimeter is shown in Fig. 4. One of the main tasks for the data analysis process is to determine the number of elastic π^0s (experimental yields) for each angular bin in the forward direction (the yellow spot in Fig. 4). Similar to the PrimEx-I experiment [11], the combination of the photon tagger with its well defined photon energy and time information together with the HyCal calorimeter defined the following event selection criteria: (1) conservation of total energy, the so called "elasticity", which is the ratio of the total energy of two photons in HyCal to the incident photon energy, $\frac{E_{\gamma\,pair}}{E_{beam}}$; (2) time difference between the HyCal and the tagger ($\sigma_t = 1.1$ ns); and (3) two photon invariant mass, $M_{\gamma\gamma}$, measured by HyCal, required to be equal to the neutral pion mass. In addition, the 3-D momentum conservation was used to determine the π^0 production angle (typically, $\sigma_\theta = 0.03°$). Two independent analysis methods have been used by two groups to extract the event yields in the PrimEx-II experiment. The goal of both methods was to minimize the non-exclusive π^0 contribution in the $M_{\gamma\gamma}$ experimental spectrum. Analysis Group I applied energy conservation to the elastically produced π^0s and their decay process, $\pi^0 \to \gamma\gamma$, to constraint the energies of the two photons, $E_{\gamma 1}$, $E_{\gamma 2}$ measured in HyCal. The narrowed $M_{\gamma\gamma}$ spectra (see Fig. 5) were fit to extract event yields (the "constraint" method). Analysis Group II projected events in the 2-D distribution of "elasticity" versus $M_{\gamma\gamma}$ onto an axis perpendicular to the kinematic correlation between elasticity and $M_{\gamma\gamma}$ to find the "hybrid" mass: $M_{Hybrid} = M_{\pi^0} + (M_{\gamma\gamma} - M_{\pi^0}\frac{E_{\gamma\,pair}}{E_{beam}})$ (the "hybrid mass" method, see Fig. 4). Both groups fitted the resulting a factor of two more sharper $M_{\gamma\gamma}$ distributions with a Gaussian plus polynomial functions to determine the π^0 yields for all angular bins.

Experimental distributions demonstrating advantages of both methods are shown in Fig. 5 together with the elasticity distribution. Background contributions from different sources (beam line, time accidentals, and from other physics processes) are also shown with different colors.

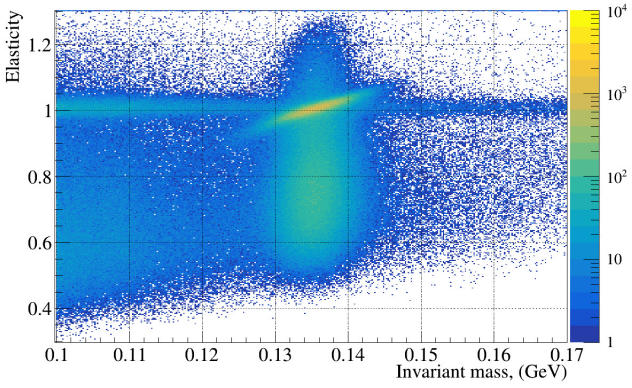

FIG. 4: 2-D distribution of experimental events in elasticity *v.s.*two photon invariant mass. The projection axes for the "hybrid mass" method are also shown with dashed lines.

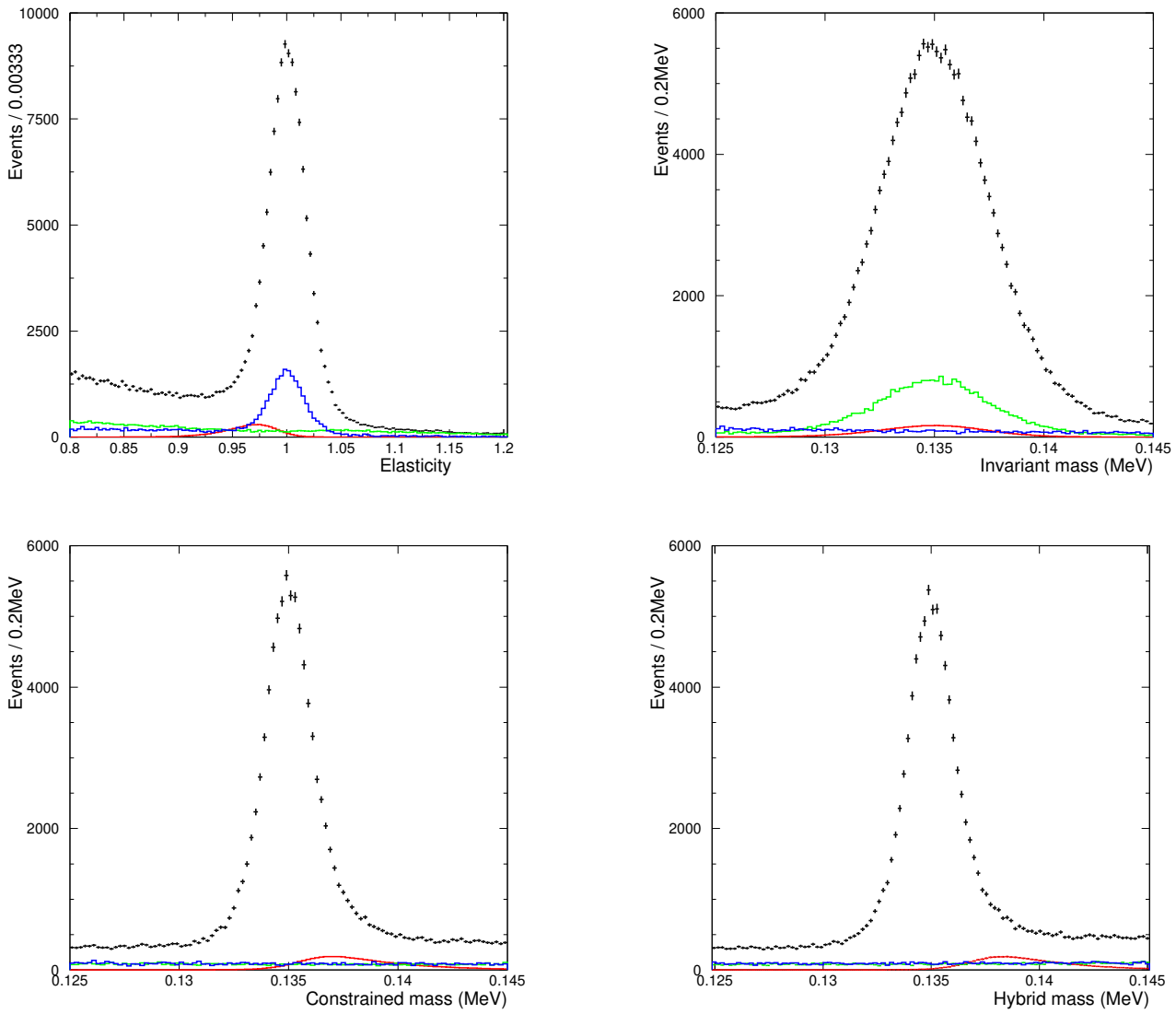

FIG. 5: Distribution of reconstructed elasticity (top left), unconstrained initial invariant mass (top right), constrained mass (bottom left) and hybrid mass (bottom right) for the ^{28}Si target and for the production angle less than one degree. Blue histograms show distributions from "empty" target run, green – time accidental events, and the red solid histograms are the Monte Carlo simulated contributions from the photoproduction of ω mesons ($\omega \to \pi^0\gamma$ channel).

TABLE I: The $\pi^0 \to \gamma\gamma$ decay widths and their uncertainties for ^{12}C and ^{28}Si targets extracted by two analysis methods.

Target	Method	$\Gamma_{\gamma\gamma}$	stat.	syst.
		eV		
^{28}Si	Hybrid	7.831	0.060	0.124
	Constrained	7.781	0.064	0.120
^{12}C	Hybrid	7.783	0.120	0.137
	Constrained	7.742	0.134	0.130

TABLE II: Breakdown of the systematic uncertainties for the PrimEx-II experiment.

Item	Contribution, [%]
Photon Flux	0.8
Yield extraction	0.8
Monte-Carlo simulation	0.55
Photoproduction parameters	0.4
Beam parameters	0.3
Target	0.3
Event selection	0.2
Total	1.4

TABLE III: Silicon cross section.

Angle, [deg.]	[μbarn/rad]	Angle, [deg.]	[μbarn/rad]
0.00-0.02	17.1±0.6	1.26-1.28	52.5±1.3
0.02-0.04	45.0±1.1	1.28-1.30	50.8±1.2
0.04-0.06	59.5±1.2	1.30-1.32	54.2±1.3
0.06-0.08	55.6±1.2	1.32-1.34	51.4±1.3
0.08-0.10	53.5±1.2	1.34-1.36	52.5±1.3
0.10-0.12	46.8±1.1	1.36-1.38	52.4±1.3
0.12-0.14	39.9±1.0	1.38-1.40	55.0±1.3
0.14-0.16	34.5±1.0	1.40-1.42	52.1±1.3
0.16-0.18	31.1±0.9	1.42-1.44	51.5±2.8
0.18-0.20	28.5±0.9	1.44-1.46	54.3±1.3
0.20-0.22	26.9±0.9	1.46-1.48	52.8±1.3
0.22-0.24	24.8±0.8	1.48-1.50	53.2±1.3
0.24-0.26	23.6±0.8	1.50-1.52	50.9±1.3
0.26-0.28	20.8±0.8	1.52-1.54	50.8±1.3
0.28-0.30	22.2±0.8	1.54-1.56	50.1±1.3
0.30-0.32	21.8±0.8	1.56-1.58	48.5±1.3
0.32-0.34	21.2±0.8	1.58-1.60	48.3±1.3
0.34-0.36	22.1±0.8	1.60-1.62	49.5±2.1
0.36-0.38	20.6±0.8	1.62-1.64	45.5±1.3
0.38-0.40	21.6±0.8	1.64-1.66	46.9±1.3
0.40-0.42	21.1±0.8	1.66-1.68	47.9±1.3
0.42-0.44	22.3±0.8	1.68-1.70	46.5±1.3
0.44-0.46	22.4±0.8	1.70-1.72	44.6±1.3
0.46-0.48	22.7±0.8	1.72-1.74	41.0±1.3
0.48-0.50	21.4±0.8	1.74-1.76	41.7±1.3
0.50-0.52	24.4±0.8	1.76-1.78	39.6±1.3
0.52-0.54	23.4±0.8	1.78-1.80	42.5±1.3
0.54-0.56	24.0±0.8	1.80-1.82	40.5±1.3
0.56-0.58	23.8±0.8	1.82-1.84	39.4±1.3
0.58-0.60	26.1±0.9	1.84-1.86	38.2±1.3
0.60-0.62	26.1±0.9	1.86-1.88	38.9±1.3
0.62-0.64	28.2±0.9	1.88-1.90	37.7±2.1
0.64-0.66	27.5±0.9	1.90-1.92	34.0±1.3
0.66-0.68	28.8±0.9	1.92-1.94	37.1±1.3
0.68-0.70	30.6±0.9	1.94-1.96	34.0±1.3
0.70-0.72	32.4±0.9	1.96-1.98	31.8±1.3
0.72-0.74	32.9±0.9	1.98-2.00	31.1±1.3
0.74-0.76	31.5±0.9	2.00-2.02	30.7±1.3
0.76-0.78	36.2±1.0	2.02-2.04	31.2±1.3
0.78-0.80	34.5±1.0	2.04-2.06	32.4±1.3
0.80-0.82	36.6±1.0	2.06-2.08	30.3±1.3
0.82-0.84	39.1±1.0	2.08-2.10	29.2±1.3
0.84-0.86	39.2±1.1	2.10-2.12	26.1±1.3
0.86-0.88	38.8±1.0	2.12-2.14	28.4±1.3
0.88-0.90	38.8±1.0	2.14-2.16	27.8±2.2
0.90-0.92	42.5±1.1	2.16-2.18	28.5±1.4
0.92-0.94	44.3±1.1	2.18-2.20	25.5±1.3
0.94-0.96	42.6±1.1	2.20-2.22	25.2±1.3
0.96-0.98	42.6±1.1	2.22-2.24	25.8±1.4
0.98-1.00	47.3±1.2	2.24-2.26	21.2±1.3
1.00-1.02	43.1±1.1	2.26-2.28	25.3±1.4
1.02-1.04	46.6±1.1	2.28-2.30	22.3±1.4
1.04-1.06	47.8±1.2	2.30-2.32	23.1±1.4
1.06-1.08	48.9±1.2	2.32-2.34	19.5±1.4
1.08-1.10	50.0±1.2	2.34-2.36	20.1±1.4
1.10-1.12	48.8±1.2	2.36-2.38	19.9±1.4
1.12-1.14	51.9±1.2	2.38-2.40	18.2±1.4
1.14-1.16	50.9±1.2	2.40-2.42	20.2±1.5
1.16-1.18	52.4±1.2	2.42-2.44	24.4±1.6
1.18-1.20	50.3±1.2	2.44-2.46	19.4±1.5
1.20-1.22	52.8±1.3	2.46-2.48	17.1±1.5
1.22-1.24	52.4±1.3	2.48-2.50	20.6±1.6
1.24-1.26	51.7±1.3	2.50-2.52	19.4±1.6

TABLE IV: Carbon cross section.

Angle, [deg.]	[μbarn/rad]	Angle, [deg.]	[μbarn/rad]
0.00-0.02	3.2±0.2	1.26-1.28	18.6±0.6
0.02-0.04	8.9±0.4	1.28-1.30	20.9±0.7
0.04-0.06	10.6±0.7	1.30-1.32	19.8±0.7
0.06-0.08	10.5±0.4	1.32-1.34	20.5±0.7
0.08-0.10	9.7±0.4	1.34-1.36	19.5±0.7
0.10-0.12	8.4±0.4	1.36-1.38	19.1±0.7
0.12-0.14	7.1±0.4	1.38-1.40	21.1±0.7
0.14-0.16	6.2±0.4	1.40-1.42	22.0±0.7
0.16-0.18	5.7±0.3	1.42-1.44	22.1±0.7
0.18-0.20	5.2±0.3	1.44-1.46	21.2±0.7
0.20-0.22	5.0±0.3	1.46-1.48	22.1±0.7
0.22-0.24	4.8±0.3	1.48-1.50	19.9±0.7
0.24-0.26	4.5±0.3	1.50-1.52	21.1±0.7
0.26-0.28	4.5±0.3	1.52-1.54	21.5±0.7
0.28-0.30	4.4±0.3	1.54-1.56	22.8±0.8
0.30-0.32	4.9±0.3	1.56-1.58	21.7±0.7
0.32-0.34	4.4±0.3	1.58-1.60	22.3±0.8
0.34-0.36	3.7±0.3	1.60-1.62	22.9±0.8
0.36-0.38	4.1±0.3	1.62-1.64	23.3±0.8
0.38-0.40	3.9±0.5	1.64-1.66	23.1±0.8
0.40-0.42	4.5±0.3	1.66-1.68	23.5±0.8
0.42-0.44	4.3±0.3	1.68-1.70	22.3±0.8
0.44-0.46	4.6±0.3	1.70-1.72	23.2±0.8
0.46-0.48	4.1±0.3	1.72-1.74	23.0±0.8
0.48-0.50	4.8±0.3	1.74-1.76	24.0±1.2
0.50-0.52	4.9±0.3	1.76-1.78	23.7±0.8
0.52-0.54	5.0±0.3	1.78-1.80	22.5±1.3
0.54-0.56	5.2±0.3	1.80-1.82	24.0±0.8
0.56-0.58	5.4±0.3	1.82-1.84	22.4±0.8
0.58-0.60	5.8±0.3	1.84-1.86	24.5±0.9
0.60-0.62	6.5±0.4	1.86-1.88	23.0±0.8
0.62-0.64	6.7±0.4	1.88-1.90	25.1±0.9
0.64-0.66	7.0±0.4	1.90-1.92	23.3±0.9
0.66-0.68	6.6±0.4	1.92-1.94	23.6±0.9
0.68-0.70	7.6±0.4	1.94-1.96	22.7±0.9
0.70-0.72	8.0±0.4	1.96-1.98	23.5±0.9
0.72-0.74	8.3±0.4	1.98-2.00	25.0±0.9
0.74-0.76	8.3±0.4	2.00-2.02	24.9±0.9
0.76-0.78	7.6±0.6	2.02-2.04	24.7±0.9
0.78-0.80	9.4±0.4	2.04-2.06	22.6±1.4
0.80-0.82	9.3±0.4	2.06-2.08	23.0±0.9
0.82-0.84	9.6±0.8	2.08-2.10	22.5±0.9
0.84-0.86	9.6±0.4	2.10-2.12	24.2±1.0
0.86-0.88	10.7±0.5	2.12-2.14	24.4±1.0
0.88-0.90	10.1±0.5	2.14-2.16	23.4±1.0
0.90-0.92	11.8±0.9	2.16-2.18	22.7±1.0
0.92-0.94	11.4±0.5	2.18-2.20	20.7±1.0
0.94-0.96	13.0±0.5	2.20-2.22	19.9±1.0
0.96-0.98	13.2±0.5	2.22-2.24	20.3±1.0
0.98-1.00	13.6±0.5	2.24-2.26	21.3±1.0
1.00-1.02	13.3±0.5	2.26-2.28	22.7±1.1
1.02-1.04	13.9±0.5	2.28-2.30	19.9±1.1
1.04-1.06	14.3±0.6	2.30-2.32	20.8±1.1
1.06-1.08	14.7±0.9	2.32-2.34	19.2±1.1
1.08-1.10	15.5±0.9	2.34-2.36	20.4±1.1
1.10-1.12	15.1±0.6	2.36-2.38	19.3±1.1
1.12-1.14	16.3±0.6	2.38-2.40	20.2±1.2
1.14-1.16	17.2±0.6	2.40-2.42	19.0±1.2
1.16-1.18	16.0±0.6	2.42-2.44	18.3±1.2
1.18-1.20	17.5±0.6	2.44-2.46	20.1±1.2
1.20-1.22	18.4±0.6	2.46-2.48	20.0±1.3
1.22-1.24	18.1±0.6	2.48-2.50	17.3±1.3
1.24-1.26	18.1±0.6	2.50-2.52	19.2±1.3